

Chapter 3

Design of a New Multi-output Constant Current Source Based on Power Allocation Control Strategy



Hongli Cheng and Lei Wang

Abstract In order to reduce the cross-regulation rate of multi-output constant current source and further improve the stability and accuracy of output current, a new design method based on power distribution control strategy is proposed. The system adopts the flyback converter as the main topology of the multi-output constant current source. The ARM system samples the real-time load value of the multi-output and combines the target current to determine the total power of the multi-output at this time. The total output power is the total input power. Ideally, combining the energy transfer of each output switch state of the multi-output flyback converter, the conduction time of the main switch transistor and the secondary side switch transistor of the flyback converter can be calculated, so as to distribute the power rationally on the transformer, thereby achieving reduced cross-regulation and improved current accuracy and stability. The experimental results show that a new multi-output constant current source system based on power distribution control has lower cross-regulation rate and the output current accuracy is within $\pm 2\%$ mA, which improves the accuracy and stability of the output current.

3.1 Introduction

At present, how to reduce the cross-regulation rate of multi-output constant current sources and improve the stability and accuracy of multi-output currents is becoming hot topic. In this regard, a lot of research and experiments have been carried out. The main reason that affects the stability and accuracy of multi-output constant current source is the existence of cross-regulation rate. The multi-output flyback converter will only use feedback regulation for the main output, while the auxiliary output will use open-loop non-feedback [1]. The reason for the deterioration of the cross-regulation rate is the non-ideality of the transformer (leakage inductance and diode drop) [2]. The literature [3] proposes a new TDK-Lambda solution to

H. Cheng · L. Wang (✉)

College of Communication and Information Engineering, Xi'an University of Science and Technology, Xi'an 710000, China
e-mail: 13149169707@163.com

© Springer Nature Singapore Pte Ltd. 2021

S.-L. Peng et al. (eds.), *Sensor Networks and Signal Processing*, Smart Innovation, Systems and Technologies 176, https://doi.org/10.1007/978-981-15-4917-5_3

improve the multi-output cross-regulation rate. The literature [4–8] proposes the use of weighted voltage feedback control method, passive lossless box circuit and optimized transformer, magnetic amplification, etc. These methods are used to improve the cross-regulation rate of the converter. Although these methods reduce the cross-regulation rate, they do not reduce the total amount of error, and the algorithm and circuit are complicated. In [9], a design method based on power distribution control strategy is proposed. This method fundamentally solves the problem of multi-output cross-regulation rate caused by the existence of leakage inductance and improves the accuracy and stability of the output voltage. However, this design method is not suitable for high-precision multi-channel constant current sources. On the one hand, the previous control strategy is multi-channel constant voltage output instead of multi-channel constant current output. On the other hand, two methods are used in the literature to prove that the multi-channel design method lacks generality, and the accuracy of multi-channel output is low. The main reason for low accuracy is that the on-time calculation of the main switch and the output switch is too simplified in the power distribution control strategy firstly. Secondly, the mutual inductance between the primary and secondary inductors of the flyback converter after the main switch transistor is turned off is not considered, so it is difficult to achieve the accuracy required by the design.

Based on the original power allocation control strategy, this paper proposes a new power distribution control-based flyback converter secondary side switch transistor on-time calculation method to reduce cross-adjustment rate for multi-channel constant current source. The control strategy further improves the current accuracy and the stability of the multi-output constant current source.

3.2 System Composition and Control Strategy

3.2.1 System Composition

The main structure of the circuit of the multi-output constant current source is shown in Fig. 3.1. If the output voltage and output current value of each channel are measured, the real-time load value of each channel and the rated output total power required for each channel can be determined. The total rated output power is equal to the input power, and the input end of the transformer determines the input power by controlling the conduction time of the primary synchronous rectifier. And the power on the transformer is distributed by controlling the conduction time of the secondary switch transistor. The system adopts multi-output flyback converter as the main topology. The primary side of the flyback converter includes the input DC power supply $U_1(t)$ and the synchronous rectifier S that controls the power level. The secondary side of the flyback converter includes three outputs corresponding synchronous rectifiers S_1 , S_2 , and S_3 , filter capacitors C_1 , C_2 , and C_3 , three output loads R_{L1} , R_{L2} , and R_{L3} . The main control part of the system uses ARM as the control

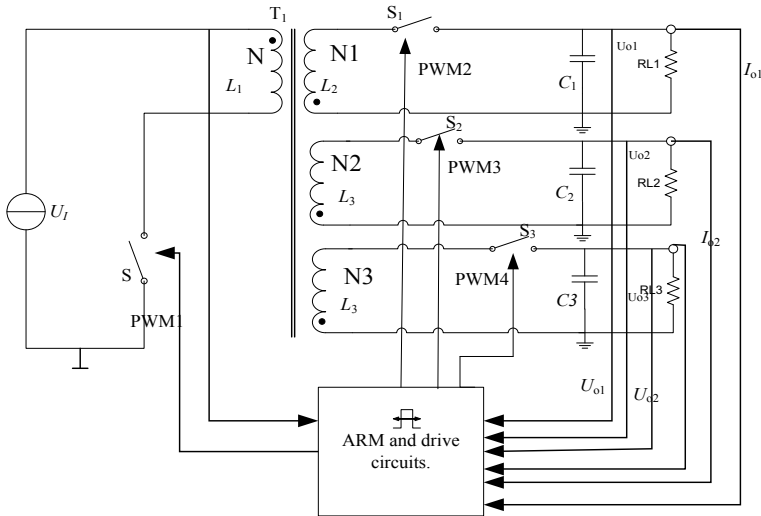


Fig. 3.1 Main circuit structure diagram of the system

core to process the collected data. The signal output by the ARM is controlled by the driving circuit to control the on and off states of several synchronous rectifiers.

ARM samples the input voltage $U_1(t)$, the output voltages $U_{o1}(t)$, $U_{o2}(t)$, and $U_{o3}(t)$, and the load currents $I_{o1}(t)$, $I_{o2}(t)$, and $I_{o3}(t)$ in real time to obtain the real-time loads R_{L1} , R_{L2} , and R_{L3} . ARM calculates the rated power of each output combined with the rated current and derives the on-time of each switch according to the new design method based on the power distribution control strategy. The ratio of the on-time to the period is four PWM waves. The requirements of the three outputs for the rated power can be satisfied by controlling the duty cycle of the four PWM waves.

3.2.2 System Control Strategy

Equation (3.1) is the real-time load value expression sampled by the ARM system. In the formula, R_{Li} is the i th real-time load value of the flyback converter output, V_{oi} is the i th output voltage value of the flyback converter, and I_{oi} is the real-time current value of the i th of the flyback converter. The three-way output real-time loads R_{L1} , R_{L2} , and R_{L3} can be calculated using Eq. (3.1).

$$R_{Li} = \frac{v_{oi}}{i_{oi}} \tag{3.1}$$

Equation (3.2) is the output rated power expression of each load of the flyback converter. In Formula (3.2), P_{oi} is the rated output power of the i th path of the flyback converter, and I_{Ei} is the target current of the i th path of the flyback converter. The real-time load obtained by Formula (3.1) can obtain the rated output power of the i th channel, and the three-way rated output power P_{o1} , P_{o2} , P_{o3} can be calculated by Formula (3.2). At this time, the total output rated power of the flyback converter is the sum of the rated output power of each output.

$$P_{oi}(t) = I_{Ei}^2 R_{Li} \quad (3.2)$$

Ideally, the total output rated power of the flyback converter is the total rated power of the input. However, the primary and secondary energy of the flyback converter cannot be completely transferred due to the leakage inductance and mutual inductance. Assume that the conversion efficiency of the high-frequency transformer, the rectifier switch, and the snubber circuit is η , and the real-time input power of the transformer is Eq. (3.3).

$$p_i(t) = \eta P_O(t) \quad (3.3)$$

The flyback converter designed by this system works in discontinuous conduction mode (DCM) [10]. According to the working principle of DCM, the input power obtained by the flyback converter is calculated as Eq. (3.4) in one switching cycle.

$$p_i(t) = \frac{U_1^2(t)t^2}{2LT} \quad (3.4)$$

In Eq. (3.4), L is the primary inductance value of the flyback converter, $U_1(t)$ is the input real-time voltage, T is the main switching period, and t is the conduction time of the main switch transistor in one switching period. According to Eqs. (3.3) and (3.4), the on-time t of the main switch S in one switching period can be obtained as Eq. (3.5).

$$t = \sqrt{\frac{P_O(t) \cdot 2LT}{\eta U_1^2(t)}} \quad (3.5)$$

Let $n_1 = N_1/N$, $n_2 = N_2/N$, $n_3 = N_3/N$, $V_{E1} = I_{E1}R_{L1}$, $V_{E2} = I_{E2}R_{L2}$, $V_{E3} = I_{E3}R_{L3}$, N , N_1 , N_2 , N_3 are the primary turns and secondary of the flyback converter, respectively. The number of turns n_1 , n_2 , and n_3 is the primary and secondary ratios of the flyback converter, respectively. I_{INMAX} is the peak value of the primary inductor current. I_{1MAX} , I_{2MAX} , and I_{3MAX} are the inductor current peaks of the first-stage secondary side, respectively. According to the above and multi-output output flyback converter ampere-conservation principle, Formulas (3.6), (3.7), and (3.8) can be obtained early.

$$I_{INMAX} = n_1 \cdot I_{1MAX} + n_2 \cdot I_{2MAX} + n_3 \cdot I_{3MAX} \quad (3.6)$$

$$\frac{I_{1MAX} \cdot I_{E1} \cdot R_{L2}}{I_{2MAX} \cdot I_{E2} \cdot R_{L2}} = \frac{N_1}{N_2} = \frac{n_1}{n_2} \quad (3.7)$$

$$\frac{I_{1MAX} \cdot I_{E1} \cdot R_{L2}}{I_{3MAX} \cdot I_{E3} \cdot R_{L3}} = \frac{N_1}{N_3} = \frac{n_1}{n_3} \quad (3.8)$$

The three peak currents of the secondary side inductance of the flyback converter obtained by Eqs. (3.6), (3.7), and (3.8) are expressed by Eqs. (3.9), (3.10), and (3.11).

$$I_{1MAX} = \frac{n_1 \cdot V_{E2} \cdot V_{E3} \cdot I_{INMAX}}{n_1^2 V_{E2} V_{E3} + n_2^2 V_{E1} V_{E3} + n_3^2 V_{E1} V_{E2}} \quad (3.9)$$

$$I_{2MAX} = \frac{n_2 \cdot V_{E1} \cdot V_{E3} \cdot I_{INMAX}}{n_1^2 V_{E2} V_{E3} + n_2^2 V_{E1} V_{E3} + n_3^2 V_{E1} V_{E2}} \quad (3.10)$$

$$I_{3MAX} = \frac{n_3 \cdot V_{E1} \cdot V_{E2} \cdot I_{INMAX}}{n_1^2 V_{E2} V_{E3} + n_2^2 V_{E1} V_{E2} + n_3^2 V_{E1} V_{E2}} \quad (3.11)$$

After the main switch transistor is turned off, the secondary side three channels simultaneously release current. When the system is operating in the first stage, the inductor current on the three secondary windings is shown in Fig. 3.2.

Assume that the three inductor currents reach their respective rated output current requirements after the times t_{s1} , t_{s2} , and t_{s3} , respectively, and the times at t_{s1} , t_{s2} , and t_{s3} can be found. According to the inductor current waveform in the first stage of Fig. 3.2. The corresponding inductor current values I_1' , I_2' , and I_3' are shown in Eq. (3.12).

$$\begin{cases} I_1' = I_{1MAX} - \frac{V_{E1}}{L_1} t_{s1} \\ I_2' = I_{2MAX} - \frac{V_{E2}}{L_2} t_{s2} \\ I_3' = I_{3MAX} - \frac{V_{E3}}{L_3} t_{s3} \end{cases} \quad (3.12)$$

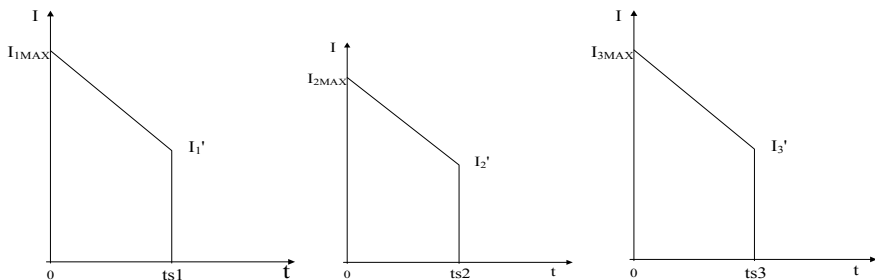


Fig. 3.2 Second-stage secondary inductance current diagram of the system

At this time, the average output current of the three channels is the rated current. The output rated current can be expressed as Eq. (3.13).

$$I_{E1} = \frac{1}{2T} (I_{1\text{MAX}} + I'_1) \cdot t_{s1} \quad (3.13)$$

$$I_{E2} = \frac{1}{2T} (I_{2\text{MAX}} + I'_2) \cdot t_{s2} \quad (3.14)$$

$$I_{E3} = \frac{1}{2T} (I_{3\text{MAX}} + I'_3) \cdot t_{s3} \quad (3.15)$$

Bringing Formula (3.12) into Eqs. (3.13), (3.14), and (3.15) can solve Eqs. (3.16), (3.17), and (3.18) when the respective outputs reach the respective rated current requirements in the first stage.

$$t_{s1} = \frac{2I_{1\text{MAX}} \cdot L_1 \pm \sqrt{4I_{1\text{MAX}}^2 L_1^2 - 8L_1 I_{E1} V_{E1} T}}{2V_{E1}} \quad (3.16)$$

$$t_{s2} = \frac{2I_{2\text{MAX}} \cdot L_2 \pm \sqrt{4I_{2\text{MAX}}^2 L_2^2 - 8L_2 I_{E2} V_{E2} T}}{2V_{E2}} \quad (3.17)$$

$$t_{s3} = \frac{2I_{3\text{MAX}} \cdot L_3 \pm \sqrt{4I_{3\text{MAX}}^2 L_3^2 - 8L_3 I_{E3} V_{E3} T}}{2V_{E3}} \quad (3.18)$$

Equations (3.16), (3.17), and (3.18) are the times when the outputs of the respective circuits reach their respective rated currents, and the on-times t_{s1} , t_{s2} , and t_{s3} of the first-stage switches are solved, and three times and minimum values are compared. It is the first turn-on time of the switch, and the remaining values are discarded. It is assumed that the on-time of the switch S_1 is the shortest at this time, and the minimum time $t = t_{s1}$ is the on-time of the corresponding switch S_1 , thereby obtaining the on-time of the switch S_1 .

The second stage is the switch with the shortest turn-off, and the other switches continue to conduct their rated current requirements. After the switch S_1 is turned off, the switches S_2 and S_3 are continuously turned on, and the other two inductor currents jump when the switch S_1 is turned off. Figure 3.3 shows the change in secondary inductor current in the second stage.

According to the change of the second stage inductor current in Fig. 3.3, the peak values of the inductor currents of the remaining paths of the first switch can be obtained as shown in Eqs. (3.19), (3.20), and (3.21).

$$I'_1 = I_{1\text{MAX}} - \frac{V_{E1}}{L_1} \cdot t_{s1} \quad (3.19)$$

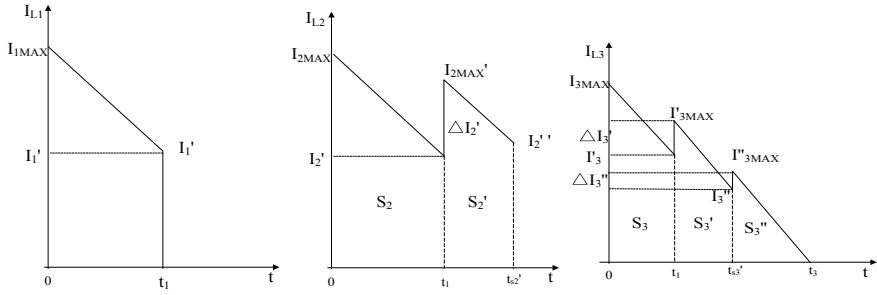


Fig. 3.3 System second-stage secondary inductor current diagram

$$I_2' = I_{2MAX} - \frac{V_{E2}}{L_2} \cdot t_{s1} \quad (3.20)$$

$$I_3' = I_{3MAX} - \frac{V_{E3}}{L_3} \cdot t_{s1} \quad (3.21)$$

$$I_{2MAX}' = I_{2MAX} - \frac{V_{E2}}{L_2} \cdot t_{s1} + \Delta I_2' \quad (3.22)$$

$$I_{3MAX}'' = I_{3MAX} - \frac{V_{E3}}{L_3} \cdot t_{s1} + \Delta I_3' \quad (3.23)$$

In Eqs. (3.22) and (3.23), $\Delta I_2'$ and $\Delta I_3'$ are transitions of the residual energy of the inductor on the inductors L_2 and L_3 .

Let $n_{21} = N_2/N_1$, $n_{31} = N_3/N_1$, and refer to Formula (3.6) to obtain:

$$I_1' = n_{21} \cdot \Delta I_2' + n_{31} \cdot \Delta I_3' \quad (3.24)$$

$$\frac{\Delta I_2' \cdot V_{E2}}{\Delta I_3' \cdot V_{E3}} = \frac{n_{21}}{n_{31}} \quad (3.25)$$

According to Eqs. (3.24) and (3.25), the jump values of the remaining two inductor currents are obtained as Eqs. (3.26) and (3.27).

$$\Delta I_2' = \frac{n_{21} \cdot V_{E3}}{n_{21}^2 V_{E3} + n_{31}^2 V_{E2}} \cdot I_1' \quad (3.26)$$

$$\Delta I_3' = \frac{n_{31} \cdot V_{E2}}{n_{21}^2 V_{E3} + n_{31}^2 V_{E2}} \cdot I_1' \quad (3.27)$$

Assume that the other two outputs reach their rated current values after the t_{s2}' , t_{s3}' time, and the expressions of the remaining two output rated currents according to Fig. 3.2 are (3.28) and (3.29).

$$I_{E2} = \frac{S_2 + [1/2(I'_{2MAX} + I'_{2MAX} - V_{E2}/L_2 \cdot (t'_{s2} - t_1)) \cdot (t'_{s2} - t_1)]}{T} \quad (3.28)$$

$$I_{E3} = \frac{S_3 + [1/2(I'_{3MAX} + I'_{3MAX} - V_{E3}/L_3 \cdot (t'_{s3} - t_1)) \cdot (t'_{s3} - t_1)]}{T} \quad (3.29)$$

According to Eqs. (3.28) and (3.29), the on-time of the switch when the remaining two paths of the second stage reach the output rated current requirement can be solved, and S_2 and S_3 are the total output current of the two channels when the first stage. Suppose $t_2 = \min\{t_{s2}', t_{s3}'\}$ is the on-time of switch S_2 , and find the value of the inductor current of the remaining two channels at time t_2 and the total output current of the second stage as Eqs. (3.30), (3.31), (3.32).

$$I''_2 = I'_{2MAX} - \frac{V_{E2}}{L_2} (t'_{s2} - t_1) \quad (3.30)$$

$$I''_3 = I'_{3MAX} - \frac{V_{E3}}{L_3} (t'_{s2} - t_1) \quad (3.31)$$

$$S'_3 = \frac{1}{2} (I'_{3MAX} + I''_3) \cdot (t'_{s2} - t_1) \quad (3.32)$$

The remaining inductor current jumps, and the system enters the third stage when the switch S_2 is turned off.

$$\Delta I'_3 = \frac{N_2}{N_3} \cdot I''_2 \quad (3.33)$$

$$I''_{3MAX} = I''_3 + \Delta I'_3 \quad (3.34)$$

$$S''_3 = \frac{1}{2} \cdot I'_{3MAX} \cdot (t'_{s3} - t_2) \quad (3.35)$$

$$I_{E3} = \frac{S_3 + S'_3 + S''_3}{T} \quad (3.36)$$

Equation (3.33) is the jump value of the inductor current at this time. Equation (3.34) is the peak value of the inductor current at time t_2 , and Eq. (3.35) is the total output current of the switch S_3 . The conduction time t'_3 of the third switch can be obtained in Eq. (3.37) by Eqs. (3.33), (3.34), (3.35), and (3.36) when the switch S_2 is turned off.

$$t'_3 = \frac{2 \cdot (I_{E3} \cdot T - S_3 - S'_3)}{I''_{3MAX}} \quad (3.37)$$

At this time, t_3 is the on-time of the switch S_3 . At this time, if $t_3 > t_{off}$, t_{off} is the main switch off time, the switch S_3 is turned on until the next cycle comes that means

the third time is as shown in Eq. (3.38).

$$t_3 = T - t \quad (3.38)$$

So far, a new three-way switch on-time of the multi-output constant current source system based on the power distribution control strategy design method is derived. The design method is based on the power allocation control strategy, and the way of calculation is accurate on the original basis. This method avoided the error caused by the inaccurate on-time of the switch conduction time.

3.3 System Programming

The ARM Cortex-M3 processor-based STM32 microcontroller is widely used for its high performance, high compatibility, easy development, and low power consumption. This design selects STM32F103RCT6 as the main control chip. It integrates a wealth of peripheral functions such as ADC, DMA, TIM, and GPIO. After frequency doubling, the system clock is 72 MHz, and two 12-bit ADC analog-to-digital conversion modules are integrated internally, which have up to 16 external signal sampling channels and can realize multi-channel data sampling. The input voltage is sampled in real time by ADC, the duty cycle of driving waveform is calculated by outputting three voltage and current values, and the timer compares and outputs four PWM signals. STM32F103RCT6 is a commonly used microcontroller of ST Company, which is suitable for: power electronic control, PWM motor drive, industrial application control, medical system, handheld equipment, PC game peripherals, GPS platform, PLC, frequency converter control, scanner, printer, alarm system, video intercom, air-conditioning heating system, and so on. This topic belongs to the application of power electronic control system, and the processing speed and function are much faster than the 51 and AVR used before. Figure 3.4 is the block diagram of the system. Firstly, the system configures the system clock and initializes each peripheral, and then the ARM samples and calculates the real-time load value after the program is initialized. Using the above derivation, the real-time output power and the on-time of each output switch transistor are calculated. The ratio of the on-time of the switch transistor to the period T is the duty ratio of each channel, and four PWM waves are output. Because the actual circuit parameters are not ideal, the primary and secondary leakage inductances of the transformer exist. The calculated secondary control PWM wave duty cycle needs to be adjusted by the program to stabilize the three output currents. The det in the flowchart is 0.01. When the flyback converter is operating, the duty cycle of the main switch is less than 0.5. Duty cycle is taken less than 0.45 to ensure that the flyback converter operates in DCM in this design.

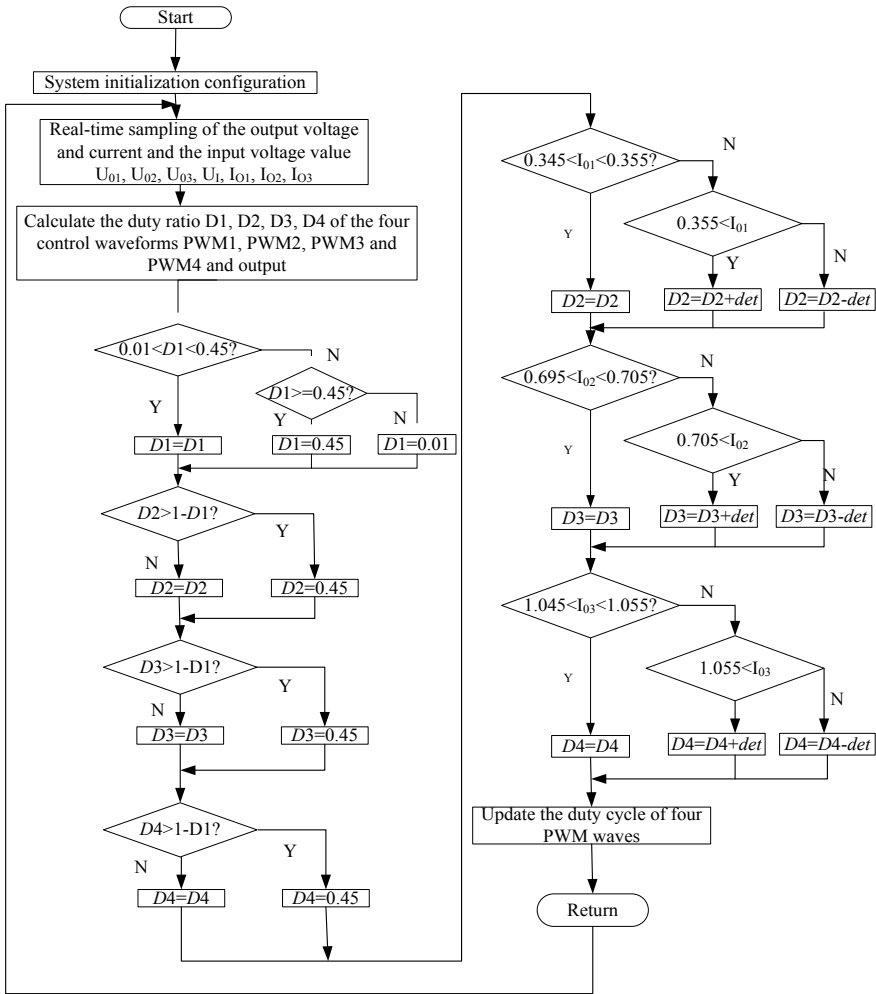


Fig. 3.4 System program flowchart

3.4 System Simulation Results Analysis

Saber simulation software is an EDA software from Synopsys of the USA. It can be used in hybrid system simulation of different types of systems such as electronics, power electronics, mechatronics, mechanical, optoelectronics, optics, and control. It provides complex mixed-signal design and verification. A powerful mixed-signal simulator is compatible with analog, digital, and control-mode hybrid simulations to solve a range of problems from system development to detailed design verification. Its main applications are power converter design, servo system design, circuit simulation, power supply and distribution design, bus simulation, and many other

fields. It has powerful and obvious advantages. The simulation of this system mainly adopts Saber.

A three-output flyback converter is designed according to the above derivation ideas and simulated by Saber.

(1) Simulation requirements

Input voltage: $U_1(t) = 60 \text{ V}$

Output power: $P_{\text{omax}} = 48 \text{ W}$

Output rated current: $I_{E1} = 0.35\text{A}; I_{E2} = 0.7\text{A}; I_{E3} = 1.05\text{A}$

Switching frequency: $f = 20 \text{ kHz}$

Maximum duty cycle: $D_{\text{max}} = 0.45$

(2) Parameter calculation

The simulation test input DC voltage $U_1(t) = 60 \text{ V}$ and the period is $50 \mu\text{s}$. The calculated primary inductance value of the flyback converter is $L_p = 250 \mu\text{H}$, the secondary inductance values $L_1 = 85 \mu\text{H}$, $L_2 = 72 \mu\text{H}$, and $L_3 = 50 \mu\text{H}$ from the literature [11–13]. The value of the output current is measured according to the load parameters listed in Table 3.1. The experimental test results are shown in Table 3.1.

Figure 3.5 is a waveform diagram of the three-way inductor current of the transformer secondary side obtained by saber simulation in the whole cycle, and Fig. 3.6 is a simulation output three-way current diagram. It can be seen that the output three-way inductor current is simultaneously released when the main switch transistor is turned off, and the other two inductor currents jump when the first switch is turned off, and the third inductor current jumps when the second switch transistor is turned off, which is consistent with the theoretical derivation. The slope of the second and third inductor currents that jump after the transition is ideally the same as the slope of the previous stage.

The Saber software is used to simulate the control method of the system. The duty cycle of the four-way PWM is calculated according to the design goal, and then the measured output current is shown in Table 3.1. According to the table calculation, when the load changes in any way, the other road loads are unchanged. The load adjustment rate of each channel does not exceed 2%, and the cross-regulation rate does not exceed 2%, which improves the cross-regulation rate. According to Table 3.1, it can be seen that when the three rated currents are 0.35, 0.7, and 1.05 A,

Table 3.1 Simulation measured database on modified power distribution control

U_1	R_{L1}	R_{L2}	R_{L3}	T (us)	t_1/T (%)	t_2/T (%)	t_3/T (%)	I_{O1} (A)	I_{O2} (A)	I_{O3} (A)
60	44	34	22	21.13	9.8	44	57.7	0.349	0.701	1.046
60	35	34	22	21.24	10.6	42.5	57.5	0.352	0.703	1.05
60	44	30	22	20.68	10.6	38.6	61	0.346	0.699	1.052
60	44	20	22	20.45	11.1	35.7	64.3	0.348	0.701	1.051
60	38	34	21	20.7	9.1	44.2	56.8	0.349	0.698	1.048
60	38	34	15	20.45	9.4	41.8	58.2	0.351	0.702	1.045

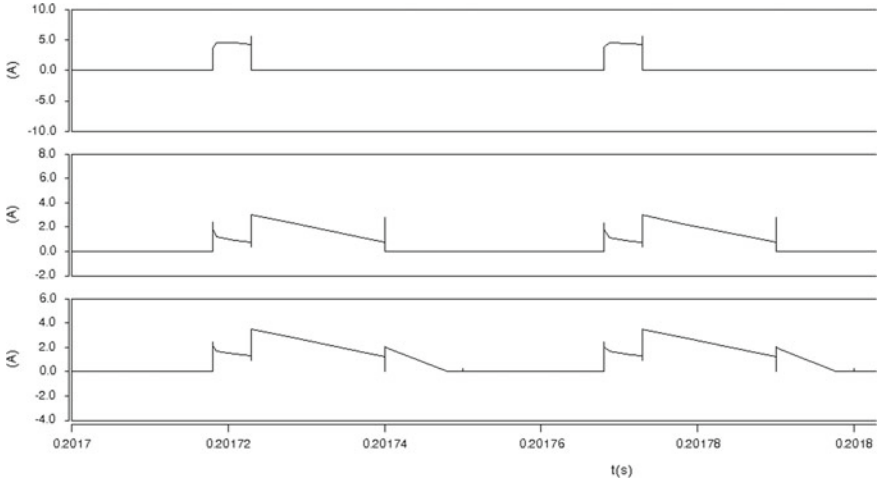


Fig. 3.5 Secondary side three-way inductor current waveform

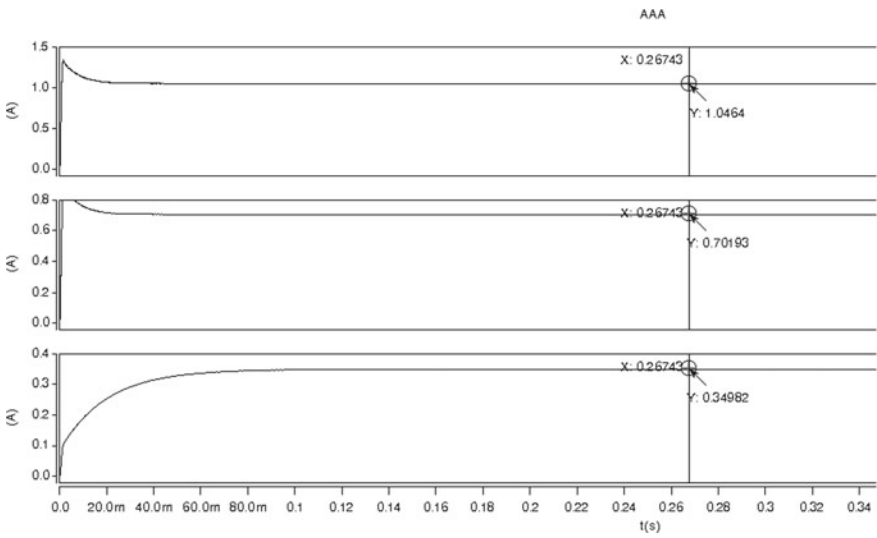


Fig. 3.6 Output current waveform measured by simulation

and the measured final output current accuracy is within $\pm 2\%$ mA, which effectively improves the accuracy of the output current. The experimental results showed that the improved method also improves the stability of multiple outputs.

3.5 Conclusion

In this paper, a new multi-output constant current source based on power distribution control strategy is designed. The system starts from the perspective of power distribution control and proposes a new method to solve the problem of cross-adjustment rate fundamentally. The design structure is simple and easy, high reliability, especially in low-power applications and low-cost multi-output power supply applications. It can meet the requirements of general multi-output power supply cross-adjustment rate. It also improved the accuracy and stability of multi-output constant current source at the same time. The overall power control is actually digital, giving the appropriate input power according to the rated power on the load and giving the appropriate power distribution according to each desired current. This paper makes the output current more accurate on the original basis by rigorous theoretical derivation. At the end of the paper, the performance parameters of the power supply are simulated and verified. The simulation results showed that the new power-based control strategy based on the secondary side conduction time is more reliable and reduced the cross-regulation rate of multiple outputs that improved the stability and accuracy of multiple output currents.

References

1. Mao, X., Chen, W.: Improving the cross-regulation rate of flyback converter by designing transformer. *Low Volt. Appar.* **2007**(23), 8–12 + 55
2. Ji, C., Smith, M., Smedley, K.M., King, K.: Cross regulation in flyback converters: analytic model and solution. *IEEE Trans. Power Electron.* **16**(2), 231–239 (2001)
3. Wang, H., Wang, Y.: A new type of solution to improve the cross-regulation rate of multi-output power supply. *Power World* **2015**(01): 25–27 + 24
4. Chen, Q., Lee, F.C., Jovanovic, M.M.: Analysis and design of weighted voltage-mode control for a multiple-output converter. *IEEE*, 449455 (1993)
5. Ji, C., Smith, M.J., Smedley, K.M.: Cross regulation in flyback converters: analytic model and solution. *IEEE Trans. Power Electron.* **16**(2), 231–239 (2001)
6. Chalermyanont, K., Sangampai, P., Prasertsit, A., Theinmontri, S.: High Frequency Transformer Designs for Improving Cross-Regulation in Multi-Output Flyback Converters. *IEEE PEDS*, pp. 53–56 (2007)
7. Jovanovic, M.M., Huber, L.: Small-signal modeling of nonideal magamp PWM switch. *IEEE Trans. Power Electron.* **14**(5), 882–889 (1999)
8. Wang, R., Wang, J., Zhang, J.: Multi-channel independent controllable constant current output LED flyback drive power supply based on post-stage adjustment. *Mech. Elect. Eng.* **33**(01), 101–105 (2016)
9. Wu, C.H., Guo, Y.J.: Multi-output flyback converter based on power distribution control. *Electron. Dev.* **40**(02), 471–475 (2017)
10. Ren, X., Ren, S., Fan, Q.: Influence of excitation current characteristics on sensor sensitivity of permeability testing technology based on constant current source. In: 2018 7th International Conference on Energy, Environment and Sustainable Development (ICEESD 2018) 2018
11. Zhao, T., Liu, H., Huang, J., et al.: Modeling and design of current mode DCM flyback converter circuit. *Power Supply Technol.* 2014(11), 2122–2124

12. Liu H, Yuan H, Shi Z, Sui S, Wang K.: Design of high precision digital AC constant current source. In: 2017 3rd International Forum on Energy, Environment Science and Materials (IFEESM 2017) (2018)
13. Zhang, Z., Cai, X.: Principle and Design of Switching Power Supply (Revised Edition). Publishing House of Electronics Industry, Beijing (2007)